Parametric Instability Analysis of Functionally Graded CNT-Reinforced Composite (FG-CNTRC) Plate Subjected to Different Types of Non-uniform In-Plane Loading

Vishal Singh, Rajesh Kumar, and Shuvendu Narayan Patel

Abstract Carbon nanotube has attracted many researchers from last two decades due to its exceptional mechanical and multiuse properties. In this article, a semi-analytical study is performed to determine the dynamic instability of a Functionally Graded Carbon Nanotube Reinforced Composite (FG-CNTRC) plate exposed to uniform and various non-uniform in-plane loadings. The efficient mechanical properties for the plate are estimated using rule of mixture where CNTs are distributed aligned and distributed across the plates' thickness such as Uniformly distributed (UD) and Functionally Graded (FG-X and FG-O). Here, The FG-CNTRC plate is modeled by means of higher order shear deformation theory (HSDT) and the stress distributions (σ_{xx}, σ_{yy}, τ_{xy}) within the plate because of non-uniform loadings are calculated using Airy's stress method. Then, the Hamilton's principle is applied to obtain the governing partial differential equations of the FG-CNTRC plate, and which is later solved with the help of Galerkin's method to convert it to ordinary (Mathieu type) differential equations. Next, these Mathieu type equations are solved employing Bolotin's method to trace the instability boundaries corresponding to period 2T. At last, the consequence of different parameters like volume fraction of CNT, types of non-uniform loading, static load factor, types of CNTs distribution on instability of the FG-CNTRC plate are examined.

Keywords FG-CNTRC · Galerkin's method · Bolotin's method · Non-uniform loading

1   Introduction

Carbon nanotubes (CNT), because of its versatile nature in different applications has drawn the attention of many investigators after its discovery by scientist Iijima (1991) and which is due to its very effective thermal, electrical, and mechanical properties (Ciecierska et al. 2013). CNTs when mixed with polymer epoxy is found to be

V. Singh · R. Kumar (✉) · S. N. Patel
Department of Civil Engineering, Birla Institute of Technology and Science, Pilani 333031, India
e-mail: rajesh.kr@pilani.bits-pilani.ac.in

increasing the strength and stiffness of the matrix (Gojny et al. 2004; Liew et al. 2015) and also increases the strength-weight and stiffness-weight ratios of the plate (Macías et al. 2017). Mehrabadi et al. (2012) and Arani et al. (2011) reported in their study that the increase in CNTs volume fraction within the matrix, increases the buckling load carrying capacity of plate. In this viewpoint, Kiani (2017) has investigated an FG-CNTRC plate loaded with parabolic loading for the analysis of buckling load, where the plate has been modeled using FSDT to approximate the kinematics of plate and solved using Ritz method and Airy stress function formulation. On similar field, Malekzadeh and Dehbozorgi (2016) works on FG-CNTRC skew plate to check its low velocity impact behavior employing first order shear deformation theory (FSDT) and solved via. finite element method (FEM) combining Newmark and Newton–Raphson methods.

It is very well understood from the above investigation that how addition of CNTs increase in strength and stiffness of the plate and which ultimately increases the buckling load carrying capacity of the plate. But estimating the buckling load and strength increment for composite plates is not only the parameters for the design of a composite plate, the effected due to dynamic loading and dynamic instability plays a important role in the design of aerospace related applications. Thus, the knowledge for dynamic stability of plate is required for proper design of composite plates. In this context CNT has some beneficial impact on the plate's dynamics stability. Rafiee et al. (2014) has investigated a piezoelectric FG-CNTRC plate with imperfection to study the nonlinear dynamic instability using FSDT and von-kármán geometric nonlinearity and solve employing Galenkin's method. Again, a temperature-dependent FG-CNTR visco-plate was analyzed for its dynamic instability behavior by Kolahchi et al. (2016) using FSDT and solved via. Generalized differential quadrature method (GDQM). In the same context, Thanh et al. (2017) has investigated nonlinear dynamic response of FG-CNTRC plate with temperature-dependent material properties using Reddy's higher order shear deformation theory (HSDT) and solved using Airy stress function, Galerkin method and fourth-order Runge–Kutta method. A dynamic instability analysis of CNTs reinforced sandwich plate under uniform in-plane loading was investigated by Sankar et al. (2016) after modeling the plate with both HSDT and FSDT, which was later solved using shear flexible QUAD-8 serendipity element. Lee (2018) performed the dynamic instability of the CNT reinforced fiber composite skew plate with delamination based on HSDT using FEM. In an investigation by Pathi and Vasudevan (2019), rotating CNT reinforced composite plate has been modeled using FSDT for the dynamic instability in the presence uniform in-plane periodic loading.

From the above literature survey, it can be predicted that study on dynamic instability of FG-CNTRC has been performed by many researchers but those were mainly oriented to uniform in-plane loading or thermal loading conditions but dynamic instability of FG-CNTRC exposed to non-uniform loading is not yet report as per the authors knowledge. The aim of this study is to investigate the dynamic instability region and behavior of UD-CNTRC and FG-CNTRC plate exposed to non-uniform in-plane loading where CNTs are aligned and distributed throughout the thickness of the plate. Mainly, the consequence of different parameters like volume

fraction of CNT, types of non-uniform loading, types of CNTs distribution, static load factor on dynamic instability of the UD-CNTRC and FG-CNTRC plate (FG-O and FG-X) are examined and the results obtained from the current work will help in appropriate design of UD-CNTRC and FG-CNTRC plate against dynamic instability under non-uniform loading conditions.

2 Formulation

In the current study, a functionally graded carbon nanotube reinforced composite (FG-CNTRC) plate is semi-analytically analyzed for dynamic instability using the formulation, as stated in this section. The constituents used in each lamina are SWCNT (chiral indices $(n_0, m_0) = (10, 10)$) and polymer matrix (epoxy resin). The effective mechanical properties of the lamina (CNT embedded matrix) are obtained using rule of mixture technique as given in next subsection. Figure 1 shows the pictorial representation of the FG-CNTRC plate and CNTs distribution across the thickness of plate.
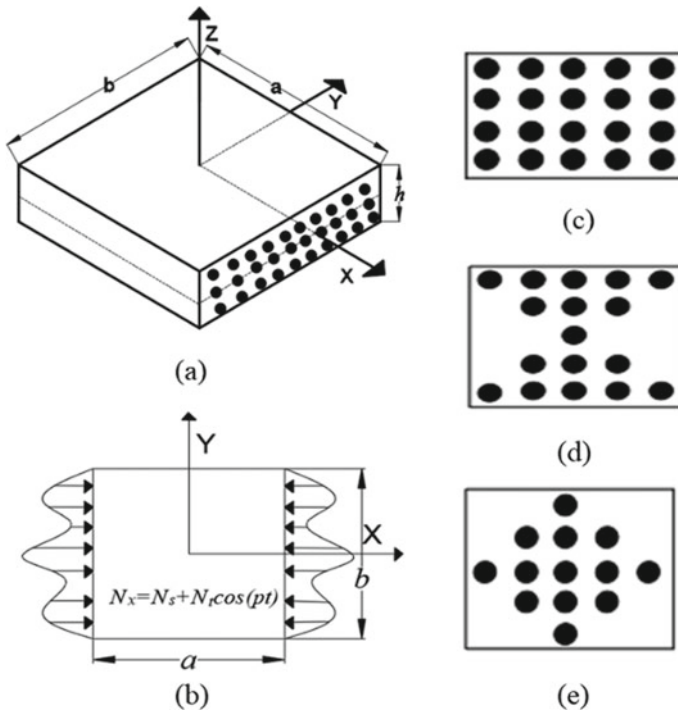
Fig. 1 Schematic view of **a** UD-CNTRC plate, **b** non-uniform loading **c** UD-CNTRC, **d** FG-X CNTRC and **e** FG-O CNTRC

Table 1 Various cases of CNTs distribution as a function thickness (Kiani 2017)

Distribution of CNTs in CNTRC plate	V_{CNT}
UD	$V_{\_cnt}$
FG-O	$2V_{\_cnt}\left(1 - 2\frac{|z|}{h}\right)$
FG-X	$4V_{\_cnt}\frac{|z|}{h}$

2.1 The Rule of Mixture

The effective mechanical properties of the FG-CNTRC plate are obtained using the rule of mixtures. However, the scale dependent properties of nanocomposite media are accounted using efficiency parameters which is mentioned in result and discussion section. According to the rule, the effective mechanical properties are estimated as:

$$E_{11} = \eta_1 V_{CNT} E_{11}^{CNT} + V_m E_m \tag{1}$$

$$\frac{\eta_2}{E_{22}} = \frac{V_{CNT}}{E_{22}^{CNT}} + \frac{V_m}{E_m} \tag{2}$$

$$\frac{\eta_3}{G_{12}} = \frac{V_{CNT}}{G_{12}^{CNT}} + \frac{V_m}{G_m} \tag{3}$$

$$V_{CNT} + V_m = 1 \tag{4}$$

$$\mu_{12} = V_{\_cnt}\mu_{11}^{CNT} + V_m\mu_m \tag{5}$$

In Eqs. (1)–(5), η_1, η_2, and η_3 are the efficiency parameters. The efficiency parameters are considered to equate the values acquired of shear modulus and Young's modulus of the current modified rule of mixtures with that of the results acquired according to the molecular dynamics simulations (Shen 2011). Besides, E_{11}^{CNT}, E_{22}^{CNT}, and G_{12}^{CNT} are the elastic moduli and shear modulus of SWCNTs, respectively. Moreover, E_m and G_m are the properties of isotropic matrix. Also, V_{CNT} and V_m denotes the volume fraction of CNTs and matrix, respectively (Kiani 2017) (Table 1).

The volume fraction of all these cases is equal to $V_{\_cnt}$ although the distribution of the CNTs are different in all cases.

2.2 Kinematics of CNTRC Plate

In the current study, the CNTRC plate is modeled considering HSDT developed by Reddy (1985). The displacement fields according to this theory, such that the

transverse shear strains at both the top and bottom surfaces are zero, for rectangular plate is as stated below:

$$u = u^0 + z\varphi_x - \frac{4z^3}{3h^2}(\varphi_x + w^0_{,x}) \tag{6}$$

$$v = v^0 + z\varphi_y - \frac{4z^3}{3h^2}(\varphi_y + w^0_{,y}) \tag{7}$$

$$w = w^0 \tag{8}$$

In the above equations, u, v, and w indicate the displacements of a material point (x, y) which is at a distance 'z' away from the neutral surface of the plate in the three principal directions. Similarly, u^0, v^0 and w^0 denote the displacements of the point on the neutral surface. φ_x and φ_y represent the rotation of the cross-section perpendicular to the x-axis and y-axis, respectively. The suffix $()_{,x}$ and $()_{,y}$ symbolize the differentiation with respect to x and y respectively. To simplify Eqs. (6) and (7), $(\varphi_x + w^0_{,x})$ is represented by ϕ^0_x and $(\varphi_y + w^0_{,y})$ is represented by ϕ^0_y. On further simplifying these equations (Eqs. 6 and 7) as per Soldatos (1991),

$$u = u^0 - zw^0_{,x} + f(z)\phi^0_x \tag{9}$$

$$v = v^0 - zw^0_{,y} + f(z)\phi^0_y \tag{10}$$

$$w = w^0 \tag{11}$$

where $f(z) = z\left(1 - \frac{4z^2}{3h^2}\right)$. At '$z$' distance ahead of the neutral surface of the plate, the strain–displacement equations can be written as:

$$\varepsilon_{xx} = \varepsilon^0_{xx} - zw^0_{,xx} + f(z)\phi^0_{x,x} \tag{12}$$

$$\varepsilon_{yy} = \varepsilon^0_{yy} - zw^0_{,yy} + f(z)\phi^0_{y,y} \tag{13}$$

$$\gamma_{xy} = \gamma^0_{xy} - 2zw^0_{,xy} + f(z)\phi^0_{x,y} + f(z)\phi^0_{y,x} \tag{14}$$

$$\gamma_{xz} = u_{,z} + w_{,x} = f'(z)\phi^0_x \tag{15}$$

$$\gamma_{yz} = v_{,z} + w_{,y} = f'(z)\phi^0_y \tag{16}$$

where, ε^0_{xx}, ε^0_{yy} and γ^0_{xy} are the strains at the neutral surface of the plate as defined in Eqs. (17)–(19).

$$\varepsilon^0_{xx} = u^0_{,x} \tag{17}$$

$$\varepsilon^0_{yy} = v^0_{,y} \tag{18}$$

$$\gamma^0_{xy} = u^0_{,x} + v^0_{,y} \tag{19}$$

According to constitutive law, the stress and strain of a lamina are related as:

$$\begin{Bmatrix} \sigma_{xx} \\ \sigma_{yy} \\ \tau_{xy} \\ \tau_{yz} \\ \tau_{xz} \end{Bmatrix} = \begin{bmatrix} Q_{11} & Q_{12} & 0 & 0 & 0 \\ Q_{12} & Q_{22} & 0 & 0 & 0 \\ 0 & 0 & Q_{66} & 0 & 0 \\ 0 & 0 & 0 & Q_{44} & 0 \\ 0 & 0 & 0 & 0 & Q_{55} \end{bmatrix} \begin{Bmatrix} \varepsilon_{xx} \\ \varepsilon_{yy} \\ \gamma_{xy} \\ \gamma_{yz} \\ \gamma_{xz} \end{Bmatrix} \tag{20}$$

where, Q_{ij} $(i, j = 1, 2, 6)$ refers to the plane stress material stiffness constants which are expressed in terms of engineering constants of CNT embedded matrix as follows:

$$Q_{11} = Q_{22} = E_{hm}/(1 - v^2_{hm}), \quad Q_{12} = v_{hm} E_{hm}/(1 - v^2_{hm}),$$
$$Q_{66} = Q_{44} = Q_{55} = E_{hm}/2(1 + v_{hm}).$$

The force, moment, and additional moment resultants in curvature due to additional changes are related to strains as defined in Eqs. (21)–(24).

$$\begin{Bmatrix} N_{xx} \\ N_{yy} \\ N_{xy} \end{Bmatrix} = \begin{bmatrix} A_{11} & A_{12} & A_{16} \\ A_{12} & A_{22} & A_{26} \\ A_{16} & A_{26} & A_{66} \end{bmatrix} \begin{Bmatrix} \varepsilon^0_{xx} \\ \varepsilon^0_{yy} \\ \gamma^0_{xy} \end{Bmatrix} + \begin{bmatrix} B_{11} & B_{12} & B_{16} \\ B_{12} & B_{22} & B_{26} \\ B_{16} & B_{26} & B_{66} \end{bmatrix} \begin{Bmatrix} -w^0_{,xx} \\ -w^0_{,yy} \\ -2w^0_{,xy} \end{Bmatrix}$$
$$+ \begin{bmatrix} C_{11} & C_{12} & C_{16} \\ C_{12} & C_{22} & C_{26} \\ C_{16} & C_{26} & C_{66} \end{bmatrix} \begin{Bmatrix} \phi^0_{x,x} \\ \phi^0_{y,y} \\ \phi^0_{x,y} + \phi^0_{y,x} \end{Bmatrix} \tag{21}$$

$$\begin{Bmatrix} M_{xx} \\ M_{yy} \\ M_{xy} \end{Bmatrix} = \begin{bmatrix} B_{11} & B_{12} & B_{16} \\ B_{12} & B_{22} & B_{26} \\ B_{16} & B_{26} & B_{66} \end{bmatrix} \begin{Bmatrix} \varepsilon^0_{xx} \\ \varepsilon^0_{yy} \\ \gamma^0_{xy} \end{Bmatrix} + \begin{bmatrix} D_{11} & D_{12} & D_{16} \\ D_{12} & D_{22} & D_{26} \\ D_{16} & D_{26} & D_{66} \end{bmatrix} \begin{Bmatrix} -w^0_{,xx} \\ -w^0_{,yy} \\ -2w^0_{,xy} \end{Bmatrix}$$
$$+ \begin{bmatrix} E_{11} & E_{12} & E_{16} \\ E_{12} & E_{22} & E_{26} \\ E_{16} & E_{26} & E_{66} \end{bmatrix} \begin{Bmatrix} \phi^0_{x,x} \\ \phi^0_{y,y} \\ \phi^0_{x,y} + \phi^0_{y,x} \end{Bmatrix} \tag{22}$$

$$
\left\{\begin{array}{c} M_{xx}^{a} \\ M_{yy}^{a} \\ M_{xy}^{a} \end{array}\right\} = \left[\begin{array}{ccc} C_{11} & C_{12} & C_{16} \\ C_{12} & C_{22} & C_{26} \\ C_{16} & C_{26} & C_{66} \end{array}\right] \left\{\begin{array}{c} \varepsilon_{xx}^{0} \\ \varepsilon_{yy}^{0} \\ \gamma_{xy}^{0} \end{array}\right\} + \left[\begin{array}{ccc} E_{11} & E_{12} & E_{16} \\ E_{12} & E_{22} & E_{26} \\ E_{16} & E_{26} & E_{66} \end{array}\right] \left\{\begin{array}{c} -w_{,xx}^{0} \\ -w_{,yy}^{0} \\ -2w_{,xy}^{0} \end{array}\right\}
$$

$$
+ \left[\begin{array}{ccc} F_{11} & F_{12} & F_{16} \\ F_{12} & F_{22} & F_{26} \\ F_{16} & F_{26} & F_{66} \end{array}\right] \left\{\begin{array}{c} \phi_{x,x}^{0} \\ \phi_{y,y}^{0} \\ \phi_{x,y}^{0} + \phi_{y,x}^{0} \end{array}\right\} \tag{23}
$$

$$
\left\{\begin{array}{c} Q_{yz}^{a} \\ Q_{xz}^{a} \end{array}\right\} = \left[\begin{array}{cc} H_{44} & H_{45} \\ H_{45} & H_{55} \end{array}\right] \left\{\begin{array}{c} \phi_{y}^{0} \\ \phi_{x}^{0} \end{array}\right\} \tag{24}
$$

where, N_{xx}, N_{yy} and N_{xy} are the force resultants; M_{xx}, M_{yy} and M_{xy} are the moment resultants; M_{xx}^{a}, M_{yy}^{a}, and M_{xy}^{a} are the additional moment resultants in curvature due to additional change, and Q_{yz}^{a} and Q_{xz}^{a} are the transverse shear force resultants. The additional change of curvature is denoted by $\phi_{x,x}^{0}$, $\phi_{y,y}^{0}$ and $\phi_{x,y}^{0} + \phi_{y,x}^{0}$. The overall CNTRC plate stiffness constants; A_{ij}, B_{ij}, C_{ij}, D_{ij}, E_{ij}, F_{ij}, and H_{ij} are expressed as stated in Eqs. (25)–(27).

$$
\left(A_{ij}, B_{ij}, D_{ij}\right) = \int_{-h/2}^{h/2} Q_{ij}\left(1, z, z^2\right) dz \quad (i, j) = (1, 2, 6) \tag{25}
$$

$$
\left(C_{ij}, E_{ij}, F_{ij}\right) = \int_{-h/2}^{h/2} Q_{ij}(1, z, f(z)) f(z) dz \quad (i, j) = (1, 2, 6) \tag{26}
$$

$$
\left(H_{ij}\right) = \int_{-h/2}^{h/2} Q_{ij} f'(z) f'(z) dz \quad (i, j) = (4, 5) \tag{27}
$$

2.3 In-Plane Elasticity Problem

It is well known that due to uniform in-plane loading at the edge of the plate, the developed pre-buckling stress distribution is also uniform and uni-axial and matches with the applied loading. However, when the non-uniform loading is applied, these three stresses components (σ_{ij}, $(i, j = x, y)$) are developed within the plate. This needs to be evaluated for estimating the internal stress resultants ((n_{ij}, $(i, j = x, y)$) due to various non-uniform loadings which are applied in-plane at the edge of the plate, to develop the governing equation of motions of the FG-CNTRC plate. The explicit analytical expressions for the pre-buckling stresses (σ_{ij}, $(i, j = x, y)$) within the FG-CNTRC plate under non-uniform in-plane mechanical loadings are developed by

solving in-plane elasticity problem using Airy's approach. Furthermore, equilibrium equation for in-plane stress in terms of Airy's stress function (ϕ) for FG-CNTRC plate is estimated using strain-compatibility conditions and is given as,

$$a_{22}\frac{\partial^4\phi}{\partial x^4} + (2a_{12} + a_{66})\frac{\partial^4\phi}{\partial x^2\partial y^2} + a_{11}\frac{\partial^4\phi}{\partial y^4} = 0 \tag{28}$$

and Airy's stress function (ϕ) is described by

$$\eta_{xx} = \frac{\partial^2\phi}{\partial y^2}, \quad \eta_{yy} = \frac{\partial^2\phi}{\partial x^2}, \quad \eta_{xy} = -\frac{\partial^2\phi}{\partial x\partial y} \tag{29}$$

where, $(A)^{-1}$ is the flexibility matrix of the FG-CNTRC plate.

$$(A)^{-1} = \begin{bmatrix} a_{11} & a_{12} & a_{16} \\ a_{12} & a_{22} & a_{26} \\ a_{16} & a_{26} & a_{66} \end{bmatrix} \tag{30}$$

Here, $A = A_{ij}$ (i, j = 1, 2, 6) is the extensional stiffness of the CNTRC plate and obtained using Eq. (25)

Now, Airy's stress function is assumed in the form of series as,

$$\phi(\text{x}, y) = \sum_{i=1}^{\infty} r_i(y)\cos(\alpha_i x) + \sum_{j=1}^{\infty} s_j(x)\cos(\beta_j y) + R_0 y^2 \tag{31}$$

where, $\alpha_i = 2i\pi/a$, $\beta_j = 2j\pi/b$, $r_i(y)$ and $s_j(x)$ are unknown functions in y and x, respectively. Substituting the above expression in the in-plane stress equilibrium Eq. (28) and then the coefficients of $\cos(\alpha_i x)$ and $\cos(\beta_j y)$ are equated which gives out the results in two ordinary differential equations in $r_i(y)$ and $s_j(x)$ respectively,

$$a_{11}\frac{\partial^4 r_i(y)}{\partial y^4} - (2a_{12} + a_{66})\alpha_i^2\frac{\partial^2 r_i(y)}{\partial y^2} + a_{22}\alpha_i^4 r_i(y) = 0 \tag{32a}$$

$$a_{22}\frac{\partial^4 s_j(x)}{\partial x^4} - (2a_{12} + a_{66})\beta_j^2\frac{\partial^2 s_j(x)}{\partial x^2} + a_{11}\beta_j^4 s_j(x) = 0 \tag{32b}$$

Substituting $r_i(y) = \exp(\overline{\lambda_2}y)$ and $s_j(x) = \exp(\overline{\lambda_1}x)$ in the above equations, roots of the above equation are $\overline{\lambda_2} = \pm\alpha_{i1}, \pm\alpha_{i2}$ and $\overline{\lambda_1} = \pm\beta_{j1}, \pm\beta_{j2}$.

Where, $\alpha_{i1}, \alpha_{i2} = \alpha_i\sqrt{\frac{(2a_{12}+a_{66})\pm\sqrt{(2a_{12}+a_{66})^2-4a_{11}a_{22}}}{a_{11}}}$ and $\beta_{j1}, \beta_{j2} = \beta_j\sqrt{\frac{(2a_{12}+a_{66})\pm\sqrt{(2a_{12}+a_{66})^2-4a_{11}a_{22}}}{a_{22}}}$. Since the functions $r_i(y)$ and $s_j(x)$ are symmetric about y and x axes respectively, we can write

$$r_i(y) = R_{i1} \cos h(\alpha_{i1} y) + R_{i2} \cos h(\alpha_{i2} y) \tag{33}$$

$$s_j(x) = S_{j1} \cos h(\beta_{j1} x) + S_{j2} \cos h(\beta_{j2} x) \tag{34}$$

Substituting the expressions for $r_i(y)$ and $s_j(x)$ in Eq. (31), the expression for Airy's stress function is written as,

$$\phi(x, y) = \sum_{i=1}^{\infty} \{R_{i1} \cos h(\alpha_{i1} y) + R_{i2} \cos h(\alpha_{i2} y)\} \cos(\alpha_i x)$$

$$+ \sum_{j=1}^{\infty} \{S_{j1} \cos h(\beta_{j1} x) + S_{j2} \cos h(\beta_{j2} x)\} \cos(\beta_j y) + R_0 y^2 \tag{35}$$

The in-plane stress resultants are determined by substituting the stress function (Eq. 35) in Eq. (29). Thus,

$$\eta_{xx} = \sum_{i=1}^{\infty} \cos(\alpha_i x) \left(R_{i1} \cos h(\alpha_{i1} y)\alpha_{i1}^2 + R_{i2} \cos h(\alpha_{i2} y)\alpha_{i2}^2\right)$$

$$- \sum_{j=1}^{\infty} \cos(\beta_j y) \left(S_{j1} \cos h(\beta_{j1} x) + S_{j2} \cos h(\beta_{j2} x)\right)\beta_j^2 + 2R_0 \tag{36}$$

$$\eta_{yy} = - \sum_{i=1}^{\infty} \cos(\alpha_i x)(R_{i1} \cos h(\alpha_{i1} y) + R_{i2} \cos h(\alpha_{i2} y))\alpha_i^2$$

$$+ \sum_{j=1}^{\infty} \cos(\beta_j y) \left(S_{j1} \cos h(\beta_{j1} x)\beta_{j1}^2 + S_{j2} \cos h(\beta_{j2} x)\beta_{j2}^2\right) \tag{37}$$

$$\eta_{xy} = \sum_{i=1}^{\infty} \sin(\alpha_i x)\alpha_i (R_{i1} \sin h(\alpha_{i1} y)\alpha_{i1} + R_{i2} \sin h(\alpha_{i2} y))\alpha_{i2}$$

$$+ \sum_{j=1}^{\infty} \sin(\beta_j y)\beta_j \left(S_{i1} \sin h(\beta_{j1} x)\beta_{j1} + S_{i2} \cos h(\beta_{j2} x)\beta_{j2}\right) \tag{38}$$

The coefficients, $R_{i1}, R_{i2}, S_{j1}, S_{j2}$ in expressions $\eta_{xx}(x, y)$, $\eta_{yy}(x, y)$ and $\eta_{xy}(x, y)$ are calculated using in-plane stress boundary conditions, which are written as

$$\eta_{xx}\left(\pm\frac{a}{2}, y\right) = R(y), \quad \eta_{xy}\left(\pm\frac{a}{2}, y\right) = 0, \quad \eta_{xy}\left(x, \pm\frac{b}{2}\right) = 0, \quad \eta_{yy}\left(x, \pm\frac{b}{2}\right) = 0 \tag{39}$$

where, $R(y)$ represents different types of in-plane non-uniform mechanical edge load distributions. Satisfying the in-plane stress boundary conditions which results in following set of simultaneous equations in the form of unknown coefficients,

$$R_{i1} = -\left(\frac{\alpha_{i2}}{\alpha_{i1}}\right)\frac{\sin h \frac{\alpha_{i2}b}{2}}{\sin h \frac{\alpha_{i1}b}{2}} R_{i1} \tag{40}$$

$$S_{j1} = -\left(\frac{\beta_{j2}}{\beta_{j1}}\right)\frac{\sin h \frac{\beta_{j2}a}{2}}{\sin h \frac{\beta_{j1}a}{2}} S_{j2} \tag{41}$$

$$\alpha_i^2 \left(\cos h \frac{\alpha_{i2}b}{2} - \frac{\alpha_{i2}}{a_{i1}} \cot h \frac{\alpha_{i1}b}{2} \sin h \frac{\alpha_{i2}b}{2}\right) R_{i2}$$
$$= -\left(\frac{2}{a}\right) \sum_{j=1}^{\infty} \frac{\beta_{j2} \cos \frac{\beta_j b}{2}}{\sin h \frac{\beta_{j1}a}{2}} \left(\beta_{j1} \sin h \frac{\beta_{j2}a}{2} I_1 - \beta_{j2} \sin h \frac{\beta_{j1}a}{2} I_2\right) S_{j2} \tag{42}$$

$$\beta_j^2 \left(\cos h \frac{\beta_{j2}a}{2} - \frac{\beta_{j2}}{\beta_{j1}} \cot h \frac{\beta_{j1}a}{2} \sin h \frac{\beta_{j2}a}{2}\right) S_{j2} + \left(\frac{2}{b}\right) I_0$$
$$= -\left(\frac{2}{b}\right) \sum_{i=1}^{\infty} \frac{\alpha_{i2} \cos \frac{\alpha_i a}{2}}{\sinh \frac{\alpha_{i1}b}{2}} \left(\alpha_{i1} \sin h \frac{\alpha_{i2}b}{2} I_3 - \alpha_{i2} \sin h \frac{\alpha_{i1}b}{2} I_4\right) R_{i2} \tag{43}$$

$$R_0 = \frac{1}{b} \int_0^{b/2} R(y) dy \tag{44}$$

Here,

$$I_0 = 2 \int_0^{b/2} R(y) \cos(\beta_j y) dy, \quad I_1 = 2 \int_0^{a/2} \cos h(\beta_{j1}x) \cos(\alpha_i x) dx,$$

$$I_2 = 2 \int_0^{a/2} \cos h(\beta_{j2}x) \cos(\alpha_i x) dx, \quad I_3 = 2 \int_0^{b/2} \cos h(\alpha_{j1}y) \cos(\beta_i y) dy,$$

$$I_4 = 2 \int_0^{b/2} \cos h(\alpha_{j2}y) \cos(\beta_j y) dy.$$

2.4 Governing Equations

Hamilton's principle Eq. (45) is employed to get the equations of motion for the FG-CNTRC plate in terms of forces, moments, additional moments and shear resultants,

$$\delta^{(1)}\left(\int_{t_0}^{t_1}(U - W - T)\right) = 0 \tag{45}$$

In the above equation, U implies strain energy, W is the external work done by the applied loads and T represents plate kinetic energy in the time interval t_0 to t_1 whereas $\delta^{(1)}$ denotes the first variation. The partial differential equations of the CNTRC plate exposed to non-uniform in-plane compressive loading (time-dependent) as follows:

$$\hat{N}_{xx,x} + \hat{N}_{xy,y} = \rho_g u^0_{,tt} \tag{46}$$

$$\hat{N}_{xy,x} + \hat{N}_{yy,y} = \rho_g v^0_{,tt} \tag{47}$$

$$M_{xx,xx} + 2M_{xy,xy} + M_{yy,yy} + \left(\hat{N}_{xx}w_{,x} + \hat{N}_{xy}w_{,y}\right)_{,x}$$
$$+ \left(\hat{N}_{xy}w_{,x} + \hat{N}_{yy}w_{,y}\right)_{,y} = \rho_g w^0_{,tt} \tag{48}$$

$$M^a_{xx,x} + M^a_{xy,y} - Q^a_{xz} = \rho_h \phi^0_{x,tt} \tag{49}$$

$$M^a_{xy,x} + M^a_{yy,y} - Q^a_{yz} = \rho_h \phi^0_{y,tt} \tag{50}$$

In the above equations, $\rho_g = \int_{-h/2}^{h/2} \rho_{hm}dz$, $\rho_h = \int_{-h/2}^{h/2} \rho_{hm}z^2dz$ and $\hat{N}_{ij} = \left[N_{ij} - n_{ij}\right]$, where $i, j = (x, y)$ and n_{ij} are the internal stress resultants due to applied non-uniform in-plane loading, and N_{ij} are the stress resultants due to the large deformation. Therefore, $\hat{N}_{ij}$ are the net stress resultants within the FG-CNTRC plate.

2.5 Galerkin's Method

The Galerkin's method is employed to minimize the error by orthogonalizing it with respect to a set of assumed basis shape function satisfying the prescribed boundary conditions. This method helps in reducing the governing partial differential equations into the set of ordinary differential equations. The displacement fields that satisfy the boundary conditions are expressed as,

$$u^0 = \sum_{m=1}^{M^*} \sum_{n=1}^{N^*} U_{mn}(t)\Theta^1_{mn}(x, y) \tag{51}$$

$$v^0 = \sum_{m=1}^{M^*} \sum_{n=1}^{N^*} V_{mn}(t)\Theta^2_{mn}(x, y) \tag{52}$$

$$w^0 = \sum_{m=1}^{M^*} \sum_{n=1}^{N^*} W_{mn}(t)\Theta^3_{mn}(x, y) \tag{53}$$

$$\phi^0_x = \sum_{m=1}^{M^*} \sum_{n=1}^{N^*} K_{mn}(t)\Theta^4_{mn}(x, y) \tag{54}$$

$$\phi^0_y = \sum_{m=1}^{M^*} \sum_{n=1}^{N^*} L_{mn}(t)\Theta^5_{mn}(x, y) \tag{55}$$

where, $U_{mn}(t)$, $V_{mn}(t)$, $W_{mn}(t)$, $K_{mn}(t)$ and $L_{mn}(t)$ are undetermined coefficients. $\Theta^1_{mn}(x, y)$, $\Theta^2_{mn}(x, y)$, $\Theta^3_{mn}(x, y)$, $\Theta^4_{mn}(x, y)$ and $\Theta^5_{mn}(x, y)$ are assumed basis functions satisfying the boundary conditions of the given problem. m and n are the numbers of modes considered in the approximate displacement fields $\left(u^0, v^0, w^o, \phi^0_x \text{ and } \phi^0_y\right)$ along x and y directions respectively. Here, the total number of terms is $5 \times M^* \times N^*$. Where, M^* and N^* are decided based on the converged solution. The simply supported boundary conditions along all the edges are considered in which only normal in-plane displacement is allowed and in-plane tangential displacements and out of plane displacements are restricted. This may be written as,

$$n_{xx} - N_{xx} = -\hat{N}_{xx}, \quad M^a_{xx} = M_{xx} = v^0 = w^0 = \phi^0_y = 0 \quad \text{at } x = -a/2, a/2$$

and

$$n_{yy} - N_{yy} = -\hat{N}_{yy}, \quad M^a_{yy} = M_{yy} = u^0 = w^0 = \phi^0_x = 0 \quad \text{at } y = -b/2, b/2.$$

The trigonometric basis functions, which satisfy the above boundary conditions at all, the edges of plate can be expressed as,

$$\Theta^1_{mn}(x, y) = \sin\left(\frac{m\pi x}{a}\right)\cos\left(\frac{n\pi y}{b}\right) \tag{56}$$

$$\Theta^2_{mn}(x, y) = \cos\left(\frac{m\pi x}{a}\right)\sin\left(\frac{n\pi y}{b}\right) \tag{57}$$

$$\Theta^3_{mn}(x, y) = \cos\left(\frac{m\pi x}{a}\right)\cos\left(\frac{n\pi y}{b}\right) \tag{58}$$

$$\Theta^4_{mn}(x, y) = \sin\left(\frac{m\pi x}{a}\right)\cos\left(\frac{n\pi y}{b}\right) \tag{59}$$

$$\Theta^5_{mn}(x, y) = \cos\left(\frac{m\pi x}{a}\right) \sin\left(\frac{n\pi y}{b}\right) \tag{60}$$

Galerkin's method implies that, $\iint_A L_i(u^o, v^o, w^o, \phi^0_x, \phi^0_y) \Theta^i_{mn}(x, y)_j dxdy = 0$ for $i = 1, 2, 3, 4, 5$ and $j = 1, 2, \ldots M^* \times N^*$ where L_i is the non-linear partial differential equations and A is the total area of the plate.

2.6 Dynamic Instability

The applied time-dependent non-uniform in-plane load is considered to be of the form $(N_x = N_s + N_t \cos(pt))$, where N_s is the static load component, N_t is the dynamic load component and 'p' denotes the excitation frequency. The dynamic instability behavior of the plate is explained by the following ordinary differential equation (i.e., Mathieu-Hill equation):

$$[M]\{\ddot{\delta}\} + [K - (N_S + N_T \cos(pt))[K_G]]\{\delta\} = \{0\} \tag{61}$$

According to Eq. (61), $[M]$ stands for mass matrix, $[K]$ stands for stiffness matrix and $[K_G]$ stands for the geometric stiffness matrix of the plate. Bolotin's method (Bolotin 1964) is employed to trace the boundaries of instability regions. In the above equations, dynamic and static loading component are varied as $N_T = \eta N_{cr}$ and $N_S = \mu N_{cr}$ such that $(\mu + \eta) \le 1$, where N_{cr} is the buckling load. The Eq. (61) has periodic solutions on the boundaries, with period $2T$. These solutions are assumed in terms of Fourier series as shown in Eqs. (62) and (63), where a_k and b_k are some arbitrary constants. In the graph of dimensionless excitation frequency (Ω) vs dynamic load factor (η), the region between curves with period $2T$ is known as the principal dynamic instability region. The region between curves of a different time period, is the region of stability.

$$\delta(t) = b_0 + \sum_{k=2,4,6}^{\infty} \left(a_k \sin\frac{kpt}{2} + b_k \cos\frac{kpt}{2}\right) \tag{62}$$

$$\delta(t) = \sum_{k=1,3,5}^{\infty} \left(a_k \sin\frac{kpt}{2} + b_k \cos\frac{kpt}{2}\right) \tag{63}$$

On substituting the above solutions of $\delta(t)$ in Eq. (61) and equating coefficients of identical sine and cosine terms, we get a homogeneous algebraic equation in terms of arbitrary constants a_k and b_k. For the solution to be non-trivial, the determinant of coefficients of a_k and b_k must be equal to zero. The equations thus obtained give the boundaries of instability. Equation (64) gives the upper and lower boundaries of the first-order approximation of principal dynamic instability region (period $2T$), while Eq. (65) gives a corrected principal instability region considering second-order

approximation.

$$\left| K^* \pm 0.5\beta N_{cr} K_G - 0.25 M p_1^2 \right| = 0 \tag{64}$$

$$\begin{bmatrix} K^* \pm 0.5\beta N_{cr} K_G & -0.5\beta N_{cr} K_G \\ -\beta N_{cr} K_G & K^{\cdot} - 2.25 M p_1^2 \end{bmatrix} - p_2^2 \begin{bmatrix} 0.25M & 0 \\ 0 & 0 \end{bmatrix} = 0 \tag{65}$$

where $K^* = [K_L] - N_S[K_G]$.

3 Result and Discussion

Following material properties is consider for the present study as per Kiani (2017). The Young's modulus (E_m) is 2.5 GPa, Mass density (ρ_m) is 1150 kg/m^3 and Poisson's ratio (μ_m) is 0.34 for matrix and for armchair single-walled carbon nanotube (SWCNT) with chiral indices ($n_0 = m_0 = 10$) having T(k) = 300, $E_{11}^{CNT} = 5.6466$ Tpa, $E_{22}^{CNT} = 7.08$ Tpa, $G_{12}^{CNT} = 1.9445$ Tpa, $\mu_{12}^{CNT} = 0.175$ $\rho_{CNT} = 1400$ kg/m^3. The efficiency parameters for three different CNTs volume fraction are: $\eta_1 = 0.137$ and $\eta_2 = 1.022$ for $V\_cnt = 0.12$, $\eta_1 = 0.142$ and $\eta_2 = 1.626$ for $V\_cnt = 0.17$, and $\eta_1 = 0.141$ and $\eta_2 = 1.585$ for $V\_cnt = 0.28$. Here, the efficiency parameter η_3 is considered equal to 0.7 η_2. The shear modulus $G_{13} = G_{12}$, whereas G_{23} is 1.2 times of G_{12}. The properties mentioned here will be used in the study further unless mentioned separately. In this section, various non-uniform in-plane edge loadings such as parabolic, concentrated, partial edge loading are considered along with uniform loading for evaluating the buckling load and boundaries of instability of the FG-CNTRC plate. The various non-uniform in-plane loading functions are given below,

Partial edge loading function is expressed as,

$$N_s = N_t = \bar{N}_0 \frac{b}{d} \left(\frac{d}{b} + \sum_{r=1}^{\infty} \frac{2}{\pi} \frac{1}{r} \sin \frac{r\pi d}{b} \cos \frac{2r\pi y}{b} \right) \tag{66}$$

Here, partial edge loading at the edge of the plate is modeled using a single Fourier series along the y-direction. In which 50 terms (i.e., $r = 1$ to 50) in Fourier series are considered for the converged pre-buckling stresses ($\sigma_{ij}, (i, j = x. y)$) within the CNTRC plate.

Parabolic loading function is expressed as,

$$N_s = N_t = \frac{3}{2} \bar{N}_0 \left(1 - 4 \frac{y^2}{b^2} \right) \tag{67}$$

Concentrated loading function is expressed as,

$$N_s = N_t = \frac{\bar{N}_0}{c\sqrt{\pi}} exp\left(-\frac{y^2}{c^2}\right) \qquad (68)$$

In this above expression, $c = 1/24$ is chosen based on converged pre-buckling stresses (σ_{ij}, ($i, j = x. y$)) within the CNTRC plate. Here, the loading function for all the different types of loadings is considered in such a way that total load (i.e., area due to the loading distribution at the edge of plate) is same.

3.1 Validation Study

To validate the accuracy and effectiveness of the current semi-analytical model, the obtained results of validation study from the present semi-analytical model along with the published one has been carried out and presented in Table 2 for the buckling load parameter $\left(k_{cr} = \frac{\lambda_{cr}b^2}{\pi^2 D}; D = \frac{E_1 h^3}{12(1-\mu_{12}^2)}\right)$ of FG-CNTRC plates exposed to parabolic in-plane edge loading $N_s = \bar{N}_0\left(1 - \frac{4y^2}{b^2}\right)$ for three cases of CNT distribution patterns, four aspect ratios with simply supported boundary conditions. The length-to-thickness ratio is chosen as $b/h = 50$, and CNTs volume fraction of set to V_cnt = 0.17. The results are well matched with the published results of Kiani (2017).

Table 3 presents the dimensionless fundamental frequencies parameter ($\Omega_n = \omega_n a^2/h\sqrt{\rho_{ep}/E_{ep}}$) of FG-CNTRC plates under uniform edge loading for three different CNT distribution patterns, three side-to-thickness ratios along with simply supported (SSSS) boundary conditions. The length-to-thickness ratio is chosen as $b/h = 50$, and the volume fraction of CNT (V_{cnt}) is considered as 0.11, 0.14 and 0.17. The results are very well matched with the published results given by Zhu et al. (2012).

The first and second (corrected) order approximation of principal instability region of a SSSS composite plate ($a/b = 1$, $b/h = 25$, 0/90/90/0, $= V_{cnt}0$) having the mechanical properties as $E_1/E_2 = 40$, $E_2 = 6.595$ GPa, $G_{12}/E_2 = 0.6$, $G_{23}/E_2 = 0.5$,

Table 2 Buckling load coefficient (k_{cr}) of FG-CNTRC plate for $V_{cnt} = 0.17$ with $b/h = 50$

Distribution	Method	a/b			
		0.8	1	1.5	2
UD	Kiani (2017)	85.8715	59.1758	32.8725	26.0732
	Present	86.4724	59.1761	32.7528	26.0783
FG-X	Kiani (2017)	122.1227	84.3354	45.5584	34.2909
	Present	123.2382	84.3704	45.3957	34.2520
FG-O	Kiani (2017)	47.4787	33.2042	20.3205	18.3286
	Present	48.0089	33.4528	20.4415	18.4381

Table 3 Comparison of dimensionless fundamental natural frequency ($\Omega_n = \omega_n a^2/h\sqrt{\rho_{ep}/E_{ep}}$) of a simply supported square plate ($a/b = 1$) with different distribution of CNTs, volume fraction of CNTs and edge-thickness ratios

| $V_{\_cnt}$			0.11		0.14		0.17	
b/h	Distribution	Method	(1,1)	(1,2)	(1,1)	(1,2)	(1,1)	(1,2)
10	UD	Zhu et al. (2012)	13.532	17.7	14.306	18.362	16.815	22.063
		Present	13.59	17.85	14.391	18.552	16.882	22.257
	FG-X	Zhu et al. (2012)	14.616	18.646	15.368	19.385	18.278	23.541
		Present	14.711	18.803	15.425	19.51	18.21	22.553
	FG-O	Zhu et al. (2012)	11.55	16.265	12.338	17.003	14.282	20.091
		Present	11.395	16.301	12.188	16.902	14.168	20.224
20	UD	Zhu et al. (2012)	17.355	21.511	18.921	22.867	21.456	26.706
		Present	17.336	21.495	18.931	22.885	21.428	26.68
	FG-X	Zhu et al. (2012)	19.939	23.776	21.642	25.359	24.735	29.809
		Present	19.935	23.763	21.621	25.335	24.631	29.665
	FG-O	Zhu et al. (2012)	13.523	18.486	14.784	19.462	16.628	22.739
		Present	13.43	18.423	14.703	19.418	16.552	22.714
50	UD	Zhu et al. (2012)	19.233	23.408	21.354	25.295	23.697	28.987
		Present	19.159	23.286	21.322	25.205	23.613	28.829
	FG-X	Zhu et al. (2012)	22.91	26.66	25.555	29.192	22.416	33.434
		Present	22.904	26.635	25.499	29.065	22.287	33.187
	FG-O	Zhu et al. (2012)	14.302	19.373	15.801	20.563	17.544	23.783
		Present	14.252	19.279	15.772	20.494	17.494	23.697

$\nu_{12} = 0.25$, $G_{13} = G_{12}$, $\nu_{13} = \nu_{12}$ is compared with the principal instability region given by Moorthy et al. (1990) in Fig. 2. It can be seen that the region of instability is in proximity to those of the result given by authors.

3.2   Influence of CNT Distribution

The dimensionless buckling load coefficient (k_{cr}) and dimensionless fundamental natural frequency (Ω_n) of the SSSS UD-CNTRC and FG-CNTRC plate for ($b/h =$
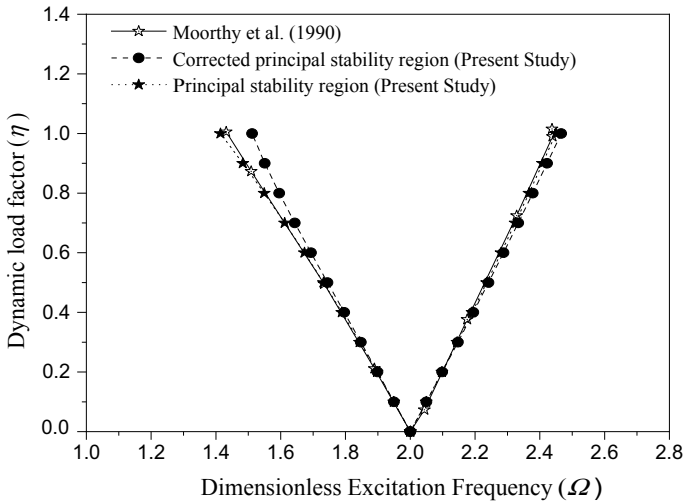
Fig. 2 Validation of principal instability region of SSSS composite plate ($a/b = 1$, $b/h = 25$, 0/90/90/0, $V_{cnt} = 0$)

20) under uniform and different types of non-uniform loadings with varying volume fraction of CNT (V_{cnt}) is given in Table 4. It can be noted from the results that the dimensionless fundamental natural frequency (Ω_n) has no effect of the types of loading applied at the edge of the plate rather it is affected by the volume fraction of CNT and type of CNT distribution over the thickness of the plate. While dimensionless buckling load coefficient (k_{cr}) is affected by both the type of loading applied at the edges of the CNTRC plate and volume fraction of CNT (V_{cnt}). It is also observed that the value of k_{cr} decreases in sequences as uniform > parabolic > partial edge ($d/b = 0.25$) > concentrated loading but rises with the increase in CNTs volume fraction, this is because the increase in CNTs volume fraction increases the stiffness of the FG-CNTRC plate while concentration of loading at the edge of the plate, decreases its stiffness. Also, the K_{cr} value of FG-X distribution is higher in comparison to K_{cr} of other two distributions, which shows that FG-X shape distribution increases the stiffness of the plate.

As per Fig. 3, the dynamic instability region (DIR) of a SSSS UD-CNTRC and FG-CNTRC plate ($a/b = 1$, $V_{cnt} = 0.17$, $b/h = 20$) under in-plane partial edge ($d/b = 0.25$) loading has been plotted for different CNT distributions with respect to the K_{cr} of FG-O. The origin of instability of FG-X distribution is having higher frequency compared to UD and FG-O type distribution, which shows that the FG-X has higher stiffness of plate than the other two. At the same time, the width of DIR at dynamic load factor $\lambda_d = 0.5$ in decreasing sequence is given as 8.17 $h\sqrt{(Eep/\rho ep)}$, 6.38$h\sqrt{(Eep/\rho ep)}$, 5.56 $h\sqrt{(Eep/\rho ep)}$ for FG-O, UD and FG-X respectively. This is because UD have uniformly distributed CNTs, FG-O has CNTs distribution as such that the top and the bottom layers have minimum and middle layer has maximum

Table 4 Dimensionless buckling load coefficient (k_{cr}) and dimensionless fundamental natural frequency (Ω_n) for different CNT distribution model of CNTRC plate ($b/h = 20$) subjected to uniform and different types of non-uniform loadings with varying volume fraction (V_{cnt})

Distribution	V_{cnt}	K_{cr}/Ω_n	Uniform	Parabolic	Partial edge ($d/b = 0.25$)	Concentrated
UD	0.12	K_{cr}	28.103	21.716	15.049	11.834
		Ω_n	15.853	15.853	15.853	15.853
	0.17	K_{cr}	42.348	32.765	22.688	18.249
		Ω_n	19.359	19.359	19.359	19.359
	0.28	K_{cr}	61.765	47.658	33.066	25.178
		Ω_n	23.113	23.113	23.113	23.113
FG-X	0.12	K_{cr}	36.774	28.418	19.692	15.500
		Ω_n	18.133	18.133	18.133	18.133
	0.17	K_{cr}	55.812	43.188	29.904	24.100
		Ω_n	22.223	22.223	22.223	22.223
	0.28	K_{cr}	78.881	60.8847	42.230	32.412
		Ω_n	26.117	26.117	26.117	26.117
FG-O	0.12	K_{cr}	17.171	13.269	9.195	7.237
		Ω_n	12.393	12.393	12.393	12.393
	0.17	K_{cr}	25.650	19.848	13.743	11.076
		Ω_n	15.067	15.067	15.067	15.067
	0.28	K_{cr}	38.080	29.392	20.387	15.647
		Ω_n	18.150	18.150	18.150	18.150
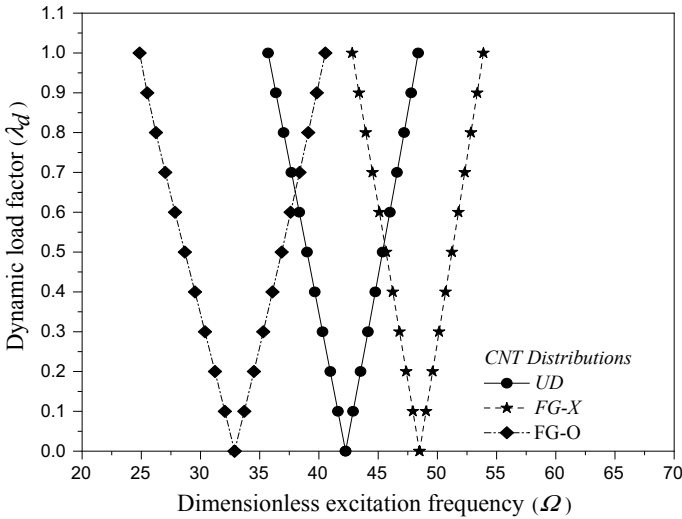
Fig. 3 Effect of CNTs distribution on principal instability zone of a SSSS UD and FG-CNTRC plate ($a/b = 1$, V_cnt $= 0.17$, $b/h = 20$) under in-plane partial edge ($d/b = 0.25$) loading
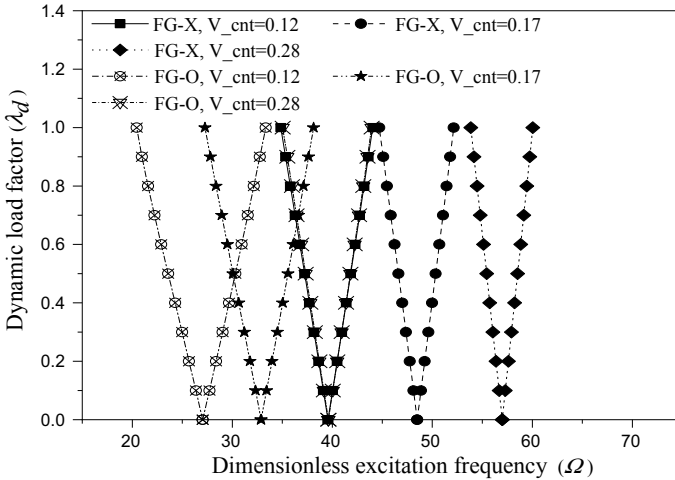
Fig. 4 Effect of type of CNTs distribution and volume fraction on principal instability zone of a SSSS FG-CNTRC plate ($a/b = 1$, $b/h = 20$) under in-plane partial edge ($d/b = 0.25$) loading

volume fraction CNTs, while, FG-X has CNTs distribution as such that the top and bottom layers have maximum and middle layer has minimum volume fraction CNTs.

In case of Fig. 4, dynamic instability region for both the types of CNTs distribution (FG-X and FG-O) are plotted with different volume fraction of CNT (V_{cnt}) for a SSSS FG-CNTRC plate ($a/b = 1$, $b/h = 20$) under in-plane partial edge (d/b = 0.25) loading with respect to the Kcr of FG-O with $V_{cnt} = 0.12$ and it is observed that the DIR of FG-X with $V_{cnt} = 0.12$ is overlapped to DIR of FG-O with $V_{cnt} = 0.28$, which signifies that the stiffness of CNTRC plate having FG-X with $V_{cnt} = 0.12$ is equal to CNTRC plate having FG-O with $V_{cnt} = 0.28$.

3.3 Influence of Various Non-uniform Loadings on Dynamic Instability Region

As per Fig. 5, it is observed that under the action of various non-uniform in-plane periodic loadings, the width of principal instability zone of a SSSS FG-X CNTRC plate ($a/b = 1$, $b/h = 20$, $V_{cnt}= 0.17$) with static load factor (λ_s) = 0 is minimum for uniform loading and maximum for concentrated loading. The width of the dynamic instability region (DIR) at dynamic load factor (λ_d) = 0.5 can be represented as $5.23h\sqrt{(Eep/\rho ep)}$, $6.75h\sqrt{(Eep/\rho ep)}$, $8.40h\sqrt{Eep/\rho ep}$, $9.73h\sqrt{Eep/\rho ep}$ and $12.05h\sqrt{(Eep/\rho ep)}$ for uniform, parabolic, partial edge ($d = 0.5$), partial edge ($d = 0.25$) and concentrated loadings respectively with respect to the buckling load of concentrated loading.
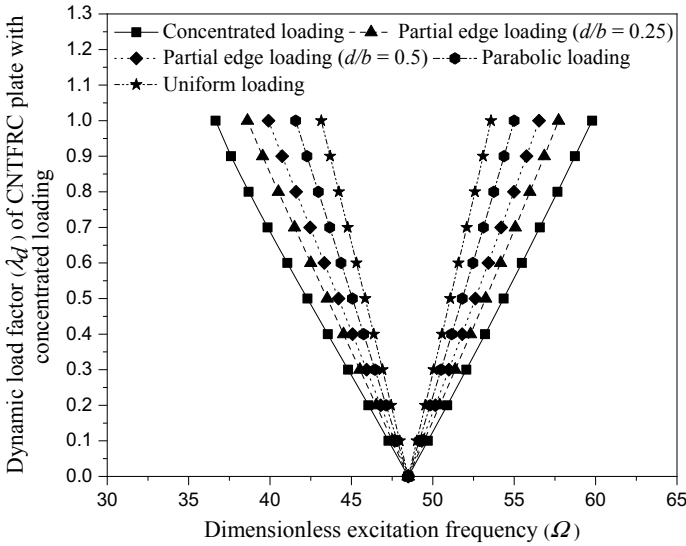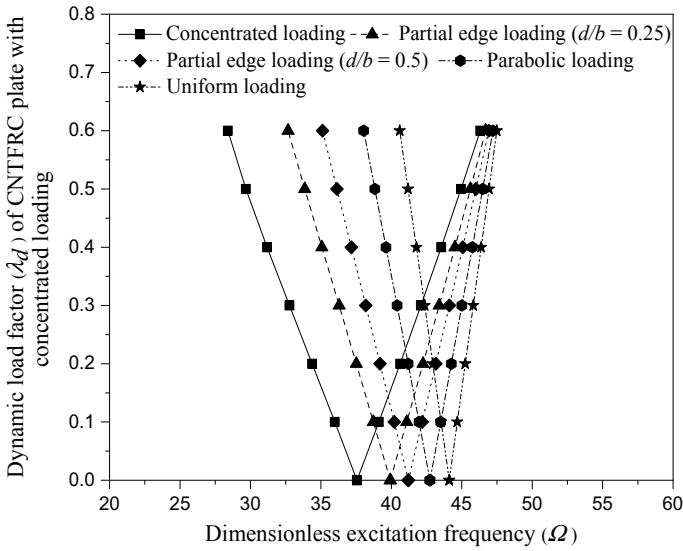
Fig. 5 Effect of different loading conditions on principal instability zone of a SSSS FG-X CNTRC Plate ($a/b = 1$, $b/h = 20$, $\lambda_s = 0$)

This reveals that with increase in concentration of loads at the edge of FG-X CNTRC plate, stiffness of the plate decreases which leads to the increase in the width of instability region. Moreover, the origin of stability region is same for all the cases of loading due to $\lambda_s = 0$. Again, from Fig. 6, it is observed that under the action of various non-uniform periodic loadings, a SSSS FG-X CNTRC plate ($a/b = 1$, $b/h = 20$, $V_{\_cnt} = 0.17$) with static load factor (λ_s) = 0.4 shows that the origin of instability region is different for every loading as compared to Fig. 5. The width of the dynamic instability region (DIR) at dynamic load factor (λ_d) = 0.5 can be represented as $5.74h\sqrt{(Eep/\rho ep)}$, $7.65h\sqrt{(Eep/\rho ep)}$, $9.86h\sqrt{Eep/\rho ep}$, $11.75h\sqrt{(Eep/\rho ep)}$ and $15.26h\sqrt{(Eep/\rho ep)}$ for uniform, parabolic, partial edge (d = 0.5), partial edge (d = 0.25) and concentrated loadings respectively with respect to the buckling load of concentrated loading.

4 Conclusion

In this article, authors have investigated the dynamic instability region of a simply supported (SSSS) FG-CNTRC plate under uniform and various types of non-uniform in-plane loadings. Here, the effect of different parameters like CNTs volume fraction, types of non-uniform loading, CNTs distribution types (UD, FG-X or FG-O), static load factor on dynamic instability of the CNTRC plate are examined. The remarks from the present investigation are summarized as,

Fig. 6 Effect of different loading conditions on principal instability zone of a simply supported FG-X CNTRC Plate ($a/b = 1$, $b/h = 20$, $\lambda_s = 0.4$)

- With the increase in CNTs volume fraction for any type of CNTs distribution in the FG-CNTRC plate, the stiffness of the plate increases which results in reducing the width of instability region.
- It was observed that the instability region for FG-X with $V_{cnt} = 0.12$ is same as the instability region of FG-O with $V_{cnt} = 0.28$. Which indicates the affect of CNT distribution on composite plate and minimization in use of volume fraction of CNT.
- Out of various loading conditions, concentrated load has maximum width of instability region and uniform loading shows minimum width of instability.

References

Arani AG, Maghamikia S, Mohammadimehr M, Arefmanesh A (2011) Buckling analysis of laminated composite rectangular plates reinforced by SWCNTs using analytical and finite element methods. J Mech Sci Technol 25(3):809–820

Bolotin VV (1964) The dynamics stabililty of elastic system. Holden day, CA, San Francisco

Ciecierska E, Boczkowska A, Kurzydlowski KJ, Rosca ID, Hoa SV (2013) The effect of carbon nanotubes on epoxy matrix nanocomposites. J Therm Anal Calorim 111:1019–1024

Gojny FH, Wichmann MHG, Köpke FB, Schulte K (2004) Carbon nanotube-reinforced epoxy-composites: enhanced stiffness and fracture toughness at low nanotube content. Compos Sci Technol 64:2363–2371

Iijima S (1991) Helical microtubules of graphitic carbon. Nature 354:56–58

Kiani Y (2017) Buckling of FG-CNT-reinforced composite plates subjected to parabolic loading. Acta Mech 228:1303–1319

Kolahchi R, Safari M, Esmailpour M (2016) Dynamic stability analysis of temperature-dependent functionally graded CNT-reinforced visco-plates resting on orthotropic elastomeric medium. Compos Struct 150:255–265

Lee SY (2018) Dynamic instability assessment of carbon nanotube/fiber/polymer multiscale composite skew plates with delamination based on HSDT. Compos Struct 200:757–770

Liew KM, Lei ZX, Zhang LW (2015) Mechanical analysis of functionally graded carbon nanotube reinforced composites: A review. Compos Struct 120:90–97

Macías EG, Tembleque LR, Triguero RC, Saez A (2017) Eshelby-Mori-Tanaka approach for post-buckling analysis of axially compressed functionally graded CNT/polymer composite cylindrical panels. Compos B 128:208–224

Malekzadeh P, Dehbozorgi M (2016) Low velocity impact analysis of functionally graded carbon nanotubes reinforced composite skew plates. Compos Struct 140:728–748

Mehrabadi SJ, Aragh BS, Khoshkhahesh V, Taherpour A (2012) Mechanical buckling of nanocomposite rectangular plate reinforced by aligned and straight single-walled carbon nanotubes. Compos B Eng 43(4):2031–2040

Moorthy J, Reddy JN, Plaut RH (1990) Parametric instability of laminated composite plates with transverse shear deformation. Int J Solids Struct 26(7):801–811

Pathi JL, Vasudevan R (2019) Numerical investigation of dynamic instability of a rotating CNT reinforced composite plate. AIP Conf Proc 2057:1–10

Rafiee M, He XQ, Liew KM (2014) Non-linear dynamic stability of piezoelectric functionally graded carbon nanotube-reinforced composite plates with initial geometric imperfection. Int J Non-Linear Mech 59:37–51

Reddy JN, Liu CF (1985) A higher-order shear deformation theory of laminated elastic shells. Int J Eng Sci 23(3):319–330

Sankar A, Natarajan S, Ganapathi M (2016) Dynamic instability analysis of sandwich plates with CNT reinforced facesheets. Compos Struct 146:187–200

Shen HS (2011) Postbuckling of nanotube-reinforced composite cylindrical shells in thermal environments, part I: axially-loaded shells. Compos Struct 93:2096–2108

Soldatos KP (1991) A refined laminated plate and shell theory with applications. J Sound Vib 144(1):109–129

Thanh NV, Khoa ND, Tuan ND, Tran P, Duc ND (2017) Nonlinear dynamic response and vibration of functionally graded carbon nanotube-reinforced composite (FG-CNTRC) shear deformable plates with temperature-dependent material properties and surrounded on elastic foundations. J Therm Stresses 40:1257–1274

Zhu P, Lei ZX, Liew KM (2012) Static and free vibration analyses of carbon nanotube-reinforced composite plates using finite element method with first order shear deformation plate theory. Compos Struct 94:1450–1460